A New Reactor for Purely Homogeneous Kinetic Studies of Endothermic Reactions

S. A. Safvi and T. J. Mountziaris
Dept. of Chemical Engineering and Center for Electronic and Electro-optic Materials,
State University of New York, Buffalo, NY 14260

A new counterflow jet reactor has been designed to study the purely homogeneous kinetics of endothermic reactions. The reactor consists of two vertical, coaxial, counterflowing, laminar jets and a radial-flow exit region. It can be used to generate a reaction zone near the stagnation point and away from walls, thus eliminating the possibility of surface reactions. One jet is heated and contains only a suitable carrier gas such as hydrogen and nitrogen, while the other is unheated and contains the compound(s) under study diluted in the same carrier gas. A 2-D model of the process has been used to simulate the thermal decomposition of tertiary-butyl-arsine, a precursor for metal-organic chemical vapor deposition of GaAs films. Performance diagrams based on Reynolds and Damköhler numbers were constructed to identify optimal operating conditions and to demonstrate the feasibility of the technique. This reactor appears to be an attractive choice for studies of the purely homogeneous kinetics of endothermic reactions at pressures close to atmospheric.

Introduction

Background

A new counterflow jet reactor has been designed for studying the purely homogeneous kinetics of endothermic reactions. The motivation for developing such a reactor stems from the need for decoupling the effects of gas-phase and surface kinetics in studies of the thermal decomposition of precursors used for metal-organic chemical vapor deposition (MOCVD) of compound semiconductors (Jensen, 1987; Kuech, 1987; Stringfellow, 1989). During MOCVD of semiconductors a mixture of precursor gases or vapors diluted in a carrier gas is passed over a heated substrate resulting in the growth of a thin solid film. A better understanding of the kinetics underlying the MOCVD process can lead to growth of high quality films and multilayer structures of compound semiconductors for advanced electronic and optoelectronic devices. It will also allow the development of predictive models of the process, which can minimize the cost of reactor optimization and scale-up by reducing the expensive and time-consuming experimental trial and error procedures that are currently being used in the microelectronics industry.

The MOCVD process involves both homogeneous reactions in the gas phase near the heated substrate and surface reactions on the substrate. A lot of effort has recently been devoted to studying these reactions. Surface reactions of precursors used for growing GaAs films have been studied under high vacuum, thus eliminating any gas-phase interactions (for example, Nishizawa et al., 1987; Donnelly et al., 1991). On the other hand, the homogeneous decomposition of such precursors has been studied in hot-wall tubular reactors (for example, Larsen et al., 1988, 1989) and in MOCVD reactors equipped with in-situ diagnostics (for example, Lee et al., 1988). However, many precursors can decompose upon heating both in the gas phase and on hot reactor surfaces, thus making the decoupling of gas phase and surface kinetics a very challenging task. Typical examples of such species are arsenic compounds, which may decompose even on inert surfaces and coat them with solid deposits that can subsequently catalyze additional decomposition reactions. For example, the thermal decomposition of arsine on glass surfaces has been found to proceed via a first-order overall reaction at 350°C (Tamaru, 1955) and more recent experiments indicate that it proceeds at lower temperatures on GaAs surfaces (Lückerath et al., 1988).

Correspondence concerning this article should be addressed to T. J. Mountziaris.

Reactor description

The proposed reactor is based on the counterflow jet concept, which has been used in the past to generate diffusion flames for studying combustion kinetics (for example, Seshadri et al., 1989) and for the synthesis of fine powders (for example, Zachariah and Semerjian, 1989). Until now only exothermic reactions have been studied using counterflowing jets. To make a counterflow jet reactor suitable for studying the purely homogeneous kinetics of endothermic reactions the configuration shown in Figure 1 is proposed. Such a reactor has been recently developed in our laboratory and was used to study the onset of the thermal decomposition of vapors of tertiary-butyl-arsine (TBA) diluted in nitrogen by mass spectrometry (Safvi and Mountziaris, 1993).

The reactor consists of two vertical, co-axial, counterflowing, laminar jets. One jet is heated and contains only a carrier gas, such as hydrogen or nitrogen, while the other is cool and contains the species under study diluted in the same carrier gas. When the two jets come in contact and a stagnation flow pattern is formed, the thermal energy of the hot jet can initiate endothermic reactions involving the species transported by the cool jet. By controlling the flow rates of the two jets and the temperature of the hot jet, the reactions are confined in a zone near the stagnation point and away from hot surfaces. The gases exit the reactor in the horizontal direction by flowing radially through a disk-shaped region.

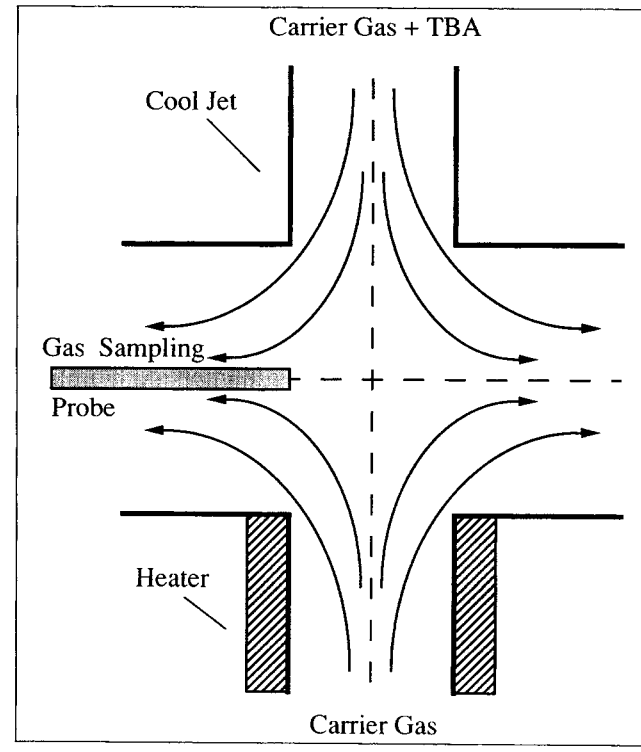

Figure 1. Counterflow jet reactor.

Gases enter by flowing through two co-axial, vertical tubes and exit by flowing radially through horizontal disk-shaped exit region. Reactor is symmetric with respect to axis of inlet tubes.

Kinetic studies

The concentrations of reactants and products in the reaction zone can be probed by mass spectrometry or by suitable optical spectroscopic techniques. The temperature of the gases can also be probed at different locations using for example low-profile thermocouples or Raman spectroscopy. The reaction zone can be shifted up or down by changing the flow rate of one of the jets. This enables the scanning of the reaction zone by a single fixed probe, if moving the probe is impractical. However, since the flow field will be different, the measurements obtained in this fashion will correspond to a different steady state. Any flow adjustments must be done within certain limits to avoid bringing the reaction zone very close to the inlet of one of the two jets, where surface reactions on walls may take place.

Under optimal operating conditions the average residence time of the reacting species in the hot zone is small enough to permit studies of the onset of its decomposition, which is typically a unimolecular reaction step. In reactors with relatively large residence times the radicals generated during unimolecular decomposition steps can subsequently attack the reactants, and the initial chemical event can be completely concealed by a complex network of very rapid secondary processes (Golden et al., 1973). One example of secondary reaction interference is the thermal decomposition of trimethyl-gallium which has been studied recently in a hot-wall tubular reactor and found to proceed faster in hydrogen than in nitrogen (Larsen et al., 1988). This observation was explained by using the secondary attack on trimethyl-gallium by the atomic hydrogen generated from the reaction of methyl radicals with the hydrogen carrier gas (Mountziaris and Jensen, 1991). The direct decomposition of trimethyl-gallium proceeds through the loss of methyl radicals by two consecutive unimolecular steps (Jacko and Price, 1963). In the reactor designed in this study, a combination of short residence times and dilute mixtures can be used to effectively suppress all secondary bimolecular reactions and allow studies of the first step of the decomposition.

The operating pressure of the reactor can be varied from atmospheric to moderate vacuum to facilitate studies of the pressure dependence of kinetic parameters. This reactor is designed to achieve at near-atmospheric pressures the ideal conditions for kinetic studies found in the classic very low pressure pyrolysis (VLPP) apparatus (Benson and Spokes, 1967; Golden et al., 1973). In the VLPP system the reactants would flow at very low pressures into a heated Knudsen cell, where they decomposed unimolecularly, and subsequently would flow molecularly through a large exit hole into the ionization chamber of a mass spectrometer, where they were analyzed directly. Arrhenius parameters for unimolecular rate constants at high pressures were obtained by using transition state theories, known as Rice-Ramsperger-Kassel (RRK) and Rice-Ramsperger-Kassel-Marcus (RRKM) theories (Robinson and Holbrook, 1972; Westmoreland et al., 1986; Roegnik et al., 1987).

The thermal decomposition of TBA was chosen as a case study in this work. TBA is a very promising arsenic precursor for MOCVD of GaAs films, because it is a liquid at room temperature and thus it is much safer to handle than the commonly used arsine gas. TBA has been successfully used for growing high quality GaAs films by MOCVD (Lum et al., 1987). Its thermal decomposition has been studied both in specially equipped MOCVD reactors (Lee et al., 1988) and in hot-wall tubular reactors (Larsen et al., 1989). The experiments

have shown that the reaction proceeds homogeneously as well as heterogeneously, especially on surfaces with strong catalytic properties, such as GaAs. When D_2 was used as the carrier gas for labeling purposes, no deuterated products were detected, which indicates that the thermal decomposition reactions of TBA do not involve the carrier gas (Larsen et al., 1989). Two parallel pathways were proposed to explain the homogeneous decomposition of TBA and their Arrhenius rate constants were estimated using data collected by mass spectrometry (Larsen et al., 1989):

(1) Intramolecular coupling to isobutane and AsH:

$$(CH_3)_3CAsH_2 \rightarrow (CH_3)_3CH + AsH;$$

$$A_1 = 1.20 \times 10^{13}\ s^{-1}, \quad E_1 = 41.5\ \text{kcal/mol}.$$

(2) β-Hydride elimination to isobutene and arsine:

$$(CH_3)_3CAsH_2 \rightarrow (CH_3)_2C{=}CH_2 + AsH_3;$$

$$A_2 = 1.74 \times 10^{14}\ s^{-1}, \quad E_2 = 48.5\ \text{kcal/mol}.$$

This simple kinetic scheme has been used in this work to demonstrate a design procedure for the counterflow jet reactor and to obtain optimal operating conditions for studying the onset of TBA decomposition.

In the following sections a model of the reactor is developed that describes flow, heat, and mass transfer. The model is used to simulate the thermal decomposition of TBA in hydrogen and nitrogen with the purpose of understanding the effects of operating conditions on the species distribution in the reactor. Performance diagrams are subsequently constructed to identify optimal operating conditions, which minimize interactions of reactants with hot surfaces. Finally, the use of the model for estimation of rate constants is discussed.

Reactor Model

A realistic steady-state model of the reactor shown in Figure 1 was developed describing momentum, heat, and mass transfer. By assuming that the mixture of the reacting species in the carrier gas is dilute, the momentum and heat-transfer problem can be decoupled from the mass-transfer and kinetics problem. For dilute mixtures the heat of reaction is negligible compared to the heat transferred by convection and conduction and any expansion or contraction of the mixture due to chemical reactions is also negligible. Under such conditions the flow and heat transfer can be studied only for the carrier gas to yield the velocity and temperature profiles in the reactor. The mass-transfer and kinetics problem can be subsequently solved to yield the species concentration profiles. For the present study, the dilute mixture assumption is reasonable for TBA concentrations below 1%, but this value may be different for other compounds.

Cylindrical coordinates have been used in the model and the computational domain with all the important geometric parameters is shown in Figure 2. The region of interest for kinetic measurements is the cylindrical region between the two jets. In the experimental reactor developed in our laboratory (Safvi and Mountziaris, 1993), the tip of a horizontal gas sampling capillary leading to a mass spectrometer is positioned along the vertical imaginary line separating the region between the jets from the exit region between the horizontal side walls (Figure 1). This imaginary line will be called the sampling line. The ranges of operating conditions covered in the present computational study are shown in Table 1.

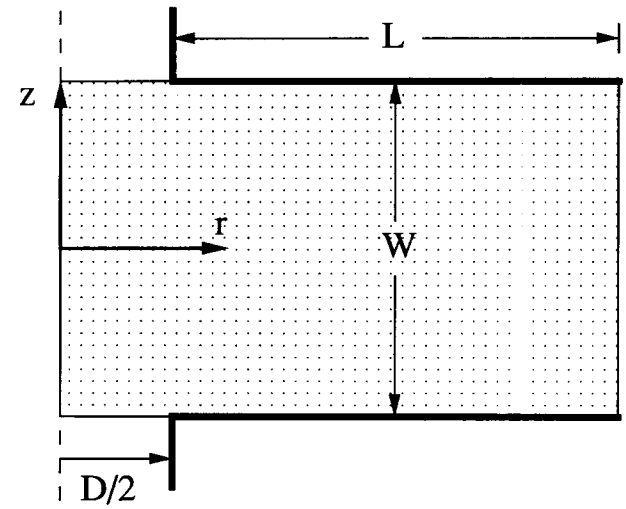

Figure 2. Computational domain (dotted region) used in simulations.

This region is bounded by reactor axis on left and exit on right. Gases enter in counterflow mode parallel to vertical axis. Vertical separation of two horizontal disks forming radial-flow exit region is W and length is L.

Flow and heat transfer

The first part of the model describes momentum and heat transfer in an ideal compressible gas. The fundamental equations of continuity, momentum, and energy balances (Bird et al., 1960) are written in dimensionless form using the diameter, D, of the inlet tubes to scale radial (horizontal) lengths, the jet separation (gap), W, to scale vertical lengths, the average upstream velocity of the cool jet, v_o, to scale velocities, the upstream inlet temperature, T_o (= 300 K), of the cool jet to scale temperatures, and the quantity $(\rho_o v_o^2)$ to scale pressures, where ρ_o is the density of the carrier gas at temperature T_o and inlet pressure p_o. The density, ρ, specific heat, c_p, viscosity, μ, and thermal conductivity, k, of the gas are scaled with their values at T_o and p_o. Then, with the assumption of no variation

Table 1. Ranges of Operating Conditions Considered in this Study

Diameter of Inlet Tube	2 cm
Gap Between Jets	1 to 4 cm
Length of Side Walls	9 cm
Temperature of Hot Jet	300 to 1,500 K
Inlet Velocity	0.8 to 140 cm/s
Operating Pressure	0.1 to 1.0 atm
Inlet Mole Fraction of TBA	0.001
Carrier Gas	H_2 or N_2
Reynolds Number	1 to 200
Damköhler Number (for TBA)	10^{-3} to 10^4

in the circumferential direction, the flow and heat-transfer model takes the following dimensionless form:

Continuity:

$$\frac{1}{r}\frac{\partial}{\partial r}(\rho r v_r)+\alpha\frac{\partial}{\partial z}(\rho v_z)=0 \tag{1}$$

r-Momentum Balance:

$$\rho\left(v_r\frac{\partial v_r}{\partial r}+\alpha v_z\frac{\partial v_r}{\partial z}\right) = -\frac{\partial p}{\partial r}+\frac{1}{Re}\left\{\frac{1}{r}\frac{\partial}{\partial r}\left\{r\mu\left[2\frac{\partial v_r}{\partial r}-\frac{2}{3}(\nabla\cdot v)\right]\right\} -\frac{\mu}{r}\left[\frac{2v_r}{r}-\frac{2}{3}(\nabla\cdot v)\right]+\alpha\frac{\partial}{\partial z}\left[\mu\left(\frac{\partial v_z}{\partial r}+\alpha\frac{\partial v_r}{\partial z}\right)\right]\right\} \tag{2}$$

z-Momentum Balance:

$$\rho\left(v_r\frac{\partial v_z}{\partial r}+\alpha v_z\frac{\partial v_z}{\partial z}\right)=-\alpha\frac{\partial p}{\partial z}+\frac{1}{Re}\left\{\frac{1}{r}\frac{\partial}{\partial r}\left[r\mu\left(\frac{\partial v_z}{\partial r}+\alpha\frac{\partial v_r}{\partial z}\right)\right] +\alpha\frac{\partial}{\partial z}\left\{\mu\left[2\alpha\frac{\partial v_z}{\partial z}-\frac{2}{3}(\nabla\cdot v)\right]\right\}\right\}-\frac{1}{Fr}\rho \tag{3}$$

where $(\nabla\cdot v)=(1/r)[\partial(rv_r)/\partial r]+\alpha(\partial v_z/\partial z)$.

Energy Balance:

$$\rho c_p\left(v_r\frac{\partial\Theta}{\partial r}+\alpha v_z\frac{\partial\Theta}{\partial z}\right) =\frac{1}{Pe}\left[\frac{1}{r}\frac{\partial}{\partial r}\left(rk\frac{\partial\Theta}{\partial r}\right)+\alpha^2\frac{\partial}{\partial z}\left(k\frac{\partial\Theta}{\partial z}\right)\right] \tag{4}$$

In the above dimensionless equations, v_r is the velocity of the gas in the radial direction, v_z is the velocity of the gas in the vertical direction, Θ is the temperature of the gas, and p is the pressure. The dimensionless numbers that appear in the equations are all evaluated using carrier gas properties at T_o and p_o. These numbers are:

(1) The Reynolds Number, $Re=(Dv_o\rho_o)/\mu_o$.
(2) The Froude Number, $Fr=v_o^2/(gD)$, where g is the gravitational acceleration.
(3) The Peclet Number for heat transfer, $Pe=(D\rho_o c_{po}v_o)/k_o$.
(4) The aspect ratio, $\alpha=D/W$.

The density of the carrier gas is connected to the pressure and temperature using the ideal gas law:

$$\rho_o=p_oM/(RT_o) \tag{5}$$

where M is the molecular weight of the carrier gas and R the ideal gas constant. Since the pressure drop in the reactor is small, the density of the gas depends only on the temperature. The dimensionless equation for the density is:

$$\rho=1/\Theta \tag{6}$$

The following dimensionless boundary conditions have been used for solving the flow and heat-transfer problem:

(1) At the axis of symmetry ($r=0$):

$$\partial v_z/\partial r=0,\quad v_r=0\quad\text{and}\quad\partial\Theta/\partial r=0 \tag{7}$$

(2) At the inlet of the cool jet ($z=+1/2$ for a cool upper jet and $r\le 1/2$):

$$v_r=0,\quad v_z=2(1-4r^2)\Theta\quad\text{and}\quad -\alpha(\partial\Theta/\partial z)=Pe(\Theta-1) \tag{8}$$

Here it is assumed that the properties of the carrier gas do not change significantly, when its temperature rises from 300 K far upstream to a higher value at the inlet of the cool jet. The pressure drop in the cool inlet tube is assumed to be negligible.

(3) At the inlet of the hot jet ($z=-1/2$ for a hot lower jet and $r\le 1/2$):

$$v_r=0,\quad v_z=2(v_{ho}/v_o)(1-4r^2)\Theta\quad\text{and}\quad\Theta=(T_h/T_o) \tag{9}$$

where v_{ho} is the average upstream velocity of the hot jet measured at 300 K and T_h is the temperature of the hot jet. The pressure drop in the hot inlet tube and any radial variations in the temperature are assumed to be negligible.

(4) Along the side walls ($z=\pm 1/2$ and $1/2\le r\le 1/2+L$): $v_r=v_z=0$ and one of the following two extreme thermal boundary conditions has been used:

$$\partial\Theta/\partial z=0\quad\text{(for an insulated wall) or}$$
$$\Theta=1\quad\text{(for a very efficiently cooled wall)} \tag{10}$$

In the second case it is assumed that the temperature of the side walls falls linearly to T_o over the first 2 cm to avoid the artifacts produced by an unrealistic step change in the temperature at the points where the side walls meet the walls of the inlet tubes.

(5) At the exit of the reactor, which is taken to be far downstream ($r=1/2+L$ and $-1/2<z<1/2$):

$$v_z=0,\quad\partial(rv_r)/\partial r=0\quad\text{and}\quad\partial\Theta/\partial r=0 \tag{11}$$

(6) Finally, the pressure was defined at one point along the exit of the reactor.

Mass transfer and kinetics

The dimensionless mass balance equation for any species i (except for the carrier gas) takes the form:

$$c\left[v_r\frac{\partial x_i}{\partial r}+v_z\frac{\partial x_i}{\partial z}\right]=\frac{1}{Pe_i}\left\{\frac{1}{r}\frac{\partial}{\partial r}\left[rcD_i\left(\frac{\partial x_i}{\partial r}+\frac{k_{Ti}}{\Theta}\frac{\partial\Theta}{\partial r}\right)\right] +\alpha^2\frac{\partial}{\partial z}\left[cD_i\left(\frac{\partial x_i}{\partial z}+\frac{k_{Ti}}{\Theta}\frac{\partial\Theta}{\partial z}\right)\right]\right\} -\sum_{j=1}^{n}\nu_{ij}\left(Da_{fj}k_{fj}c^{m_{fj}}\prod_{i=1;\,\nu_{ij}>0}^{N}x_i^{\nu_{ij}}-Da_{bj}k_{bj}c^{m_{bj}}\prod_{i=1;\,\nu_{ij}<0}^{N}x_i^{-\nu_{ij}}\right) \tag{12}$$

Table 2. Thermal Conductivity, Specific Heat and Viscosity of Carrier Gases

Gas	Thermal Conductivity (cal/cm·s·K)	Specific Heat (cal/g·K)	Viscosity (cp)
H_2	$1.779\times10^{-4}+9.03\times10^{-7}\ T(K)$	$3.284+4.02\times10^{-4}\ T(K)$	$0.0085\times[T(K)/273.15]^{0.65}$
N_2	$2.600\times10^{-5}+1.30\times10^{-7}\ T(K)$	$0.232+3.57\times10^{-5}\ T(K)$	$0.0180\times[T(K)/273.15]^{0.63}$

Here c is the dimensionless total concentration in the gas phase normalized with $c_o=\rho_o/M$, x_i is the mole fraction of the species i, D_i is the binary diffusion coefficient of the species i normalized with the diffusion coefficient D_{oi} at T_o and 1 atm, Pe_i is the Peclet number for mass transfer of species i ($Pe_i=Dv_o/D_{oi}$) and k_{Ti} is the thermal diffusion ratio for species i. The reaction term is written for a total of N species participating in n reactions. The subscript f refers to forward reactions and the subscript b to backward reactions. The stoichiometric coefficient of the ith species in the jth reaction is denoted by ν_{ij} and is taken to be positive for reactants and negative for products. The dimensionless rate coefficients of the jth reaction, k_{fj} and k_{bj}, have been normalized with their value k_{hj} computed at the average temperature $(T_o+T_h)/2$. The exponent m_j represents the order of the jth reaction and Da_j is the Damköhler number of the jth reaction defined as:

$$Da_j=\frac{k_{hj}c_o^{(m_j-1)}D}{v_o} \tag{13}$$

The reaction rate constants are assumed to be of the Arrhenius type, that is, equal to $A_j\exp(-E_j/RT)$. The mass-transfer problem involves $N-1$ partial differential equations similar to Eq. 12 and an overall mass balance for the carrier gas (Nth species):

$$x_N=1-\sum_{i=1}^{N-1}x_i \tag{14}$$

The dimensionless boundary conditions for the mass transfer of species i are:

(1) At the axis of symmetry ($r=0$):

$$\partial x_i/\partial r=0 \tag{15}$$

(2) At the inlet of the cool jet ($z=+1/2$ for a cool upper jet and $r\le1/2$):

$$-\alpha(\partial x_i/\partial z)=Pe_i(x_i-x_{io}) \tag{16}$$

where x_{io} is the known inlet concentration of species i.

(3) At the inlet of the hot jet ($z=-1/2$ for a hot lower jet and $r\le1/2$):

$$\alpha D_i(\partial x_i/\partial z)=Pe_i(v_{ho}/v_o)x_i \tag{17}$$

(4) Along the side walls ($z=\pm1/2$ and $1/2\le r\le1/2+L$):

$$\partial x_i/\partial z+(k_{Ti}/\Theta)(\partial\Theta/\partial z)=0 \tag{18}$$

(5) At the exit of the reactor ($r=1/2+L$ and $-1/2<z<1/2$), which is taken to be far downstream:

$$\partial x_i/\partial r=0 \tag{19}$$

Physical and transport properties of gaseous species

Two carrier gases were considered in this study: H_2 and N_2. Their densities were computed using the ideal gas law. Experimental values of the thermal conductivity, specific heat and viscosity of the carrier gases (Perry and Chilton, 1974) were fitted to obtain the functions of temperature listed in Table 2. Binary diffusion coefficients of AsH_3 and i-C_4H_{10} in H_2 were estimated from Lennard-Jones parameters reported in the literature (Bird et al., 1960; Reid et al., 1977). The diffusivity of TBA vapors, AsH and i-C_4H_8 in H_2 and N_2 and

Table 3. Binary Diffusion Coefficients* in Hydrogen and Nitrogen (Second Line), Lennard-Jones Parameters (σ, ϵ/κ), and Thermal Diffusion Constants in Hydrogen and Nitrogen (Second Line) for All the Species**

Species	D_o (cm²/s)	σ(Å)	ϵ/κ (K)	C_0	C_1 (K^{-1})	C_2 (K^{-2})
i-C_4H_8	0.40654	5.308	306.20	0.55177	0.11911e-02	−0.5767e-06
	0.10237			0.07058	0.48880e-03	−0.2319e-06
i-C_4H_{10}	0.39596	5.341	313.00	0.54942	0.12183e-02	−0.5890e-06
	0.09950			0.06982	0.51950e-03	−0.2464e-06
AsH	0.58689	3.890	282.30	0.40309	0.79068e-03	−0.3852e-06
	0.13533			0.07333	0.41916e-03	−0.1993e-06
AsH_3	0.55680	4.145	259.80	0.45419	0.81268e-03	−0.3987e-06
	0.12890			0.09177	0.43912e-03	−0.2091e-06
$(CH_3)_3CAsH_2$	0.32615	6.040	389.50	0.56094	0.16801e-02	−0.8020e-06
	0.07753			0.05109	0.11894e-02	−0.5625e-06

* The binary diffusion coefficient of species i in the carrier gas is equal to: $[D_{oi}\ (T/300)^{1.75}/p_r]$, where T is the temperature in K and p_r the reactor pressure in atm.
** Thermal diffusion ratio of species i (for a dilute system): $k_{Ti}=\alpha_{Ti}x_i$, where x_i is the mole fraction of species i and $\alpha_{Ti}=C_{0i}+C_{1i}T+C_{2i}T^2$, where T is the temperature in K.

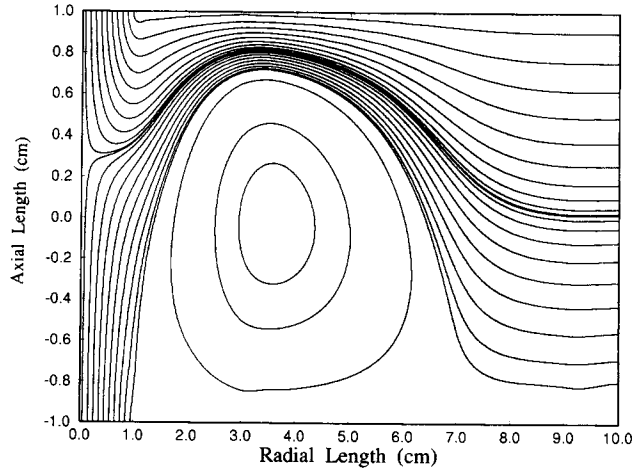

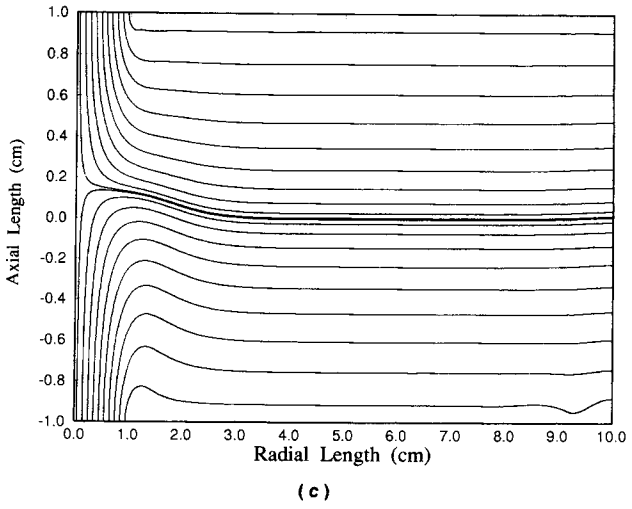

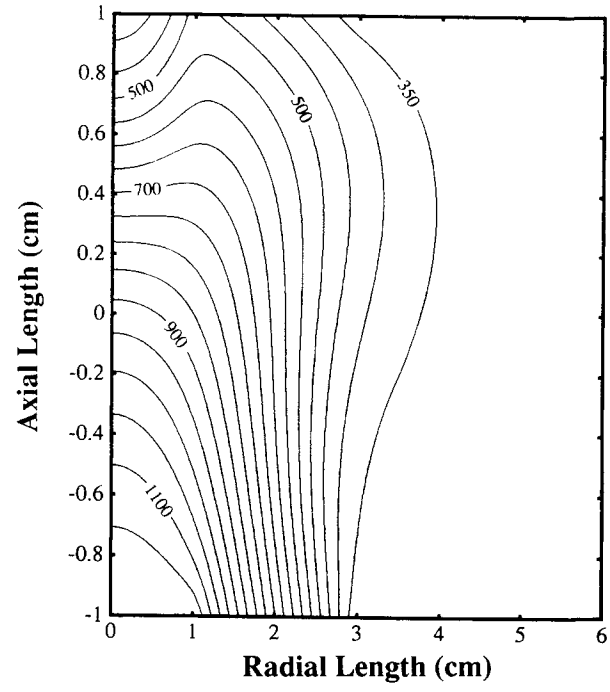

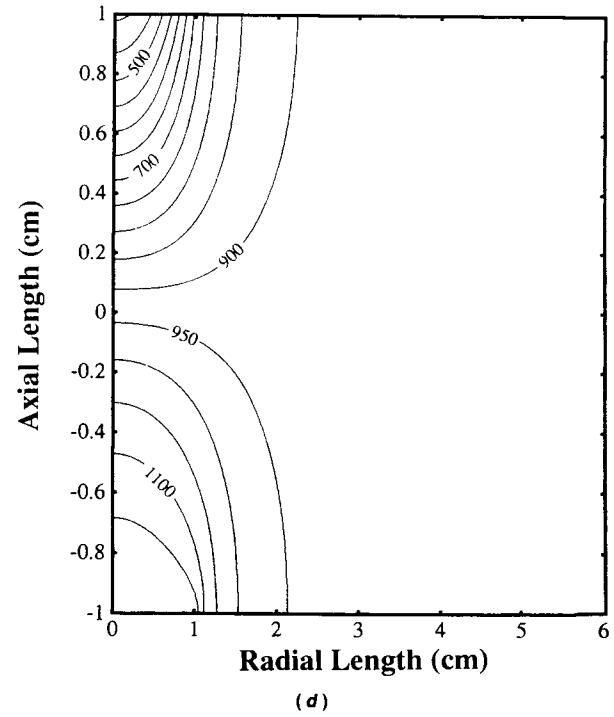

Figure 3. Pathlines (a,c) and isotherms (b,d) for hydrogen carrier gas and different side wall cooling conditions.

(a) and (b) are for cool side walls (at 300 K); (c) and (d) are for insulated side walls; all other operating conditions are same. Isotherms are plotted every 50 K; operating pressure is 1 atm. Average inlet velocity of both jets (at 300 K and 1 atm) is 5 cm/s; temperature of hot jet is 1,200 K. Reactor size: $D=2$ cm, $W=2$ cm, and $L=9$ cm. Hot jet is the lower one.

their Lennard-Jones parameters were estimated using group contribution methods (Mountziaris et al., 1993). The thermal diffusion ratio of the above species in H_2 and N_2 was estimated from their Lennard-Jones parameters (Hirschfelder et al., 1967). The values of the binary diffusion coefficients, Lennard-Jones parameters, and thermal diffusion ratios of all the gaseous species used in this study are listed in Table 3.

Numerical solution

The system of partial differential equations describing flow and heat transfer in two dimensions (axial and radial) was solved using the Galerkin finite-element method (Strang and Fix, 1973). Biquadratic elements were used for velocities and temperature, and bilinear elements for the pressure. The system of partial differential and algebraic equations describing mass-transfer and chemical reactions was subsequently solved using the same mesh and the values of gas velocities, temperatures, and pressures obtained from the flow and heat-transfer solution. Biquadratic elements were used for concentrations. A typical mesh consisted of 345 rectangular elements with 120 equally-sized elements placed in the region between the two

jets (8 in the radial direction and 15 in the vertical direction) and 225 elements in the exit region (15 in the radial direction and 15 in the vertical direction). The size of the elements was larger near the exit region where temperature and concentration gradients are small.

The system of nonlinear algebraic equations obtained after the application of Galerkin's technique was solved by using Newton's method. The computations were performed on a Cray C90 supercomputer and they typically required 19 CPU s per run for the flow and heat-transfer problem and 22 CPU s per run for the mass-transfer and kinetics problem. A series of runs was initiated using a cool isothermal reactor, where no conversion of the reactant is expected. This allowed the generation of a good initial guess for the unknown variables. Continuation on the temperature was subsequently employed to obtain solutions at higher hot jet temperatures.

The code was tested by simulating several simple cases and comparing its predictions with exact or approximate analytical solutions. The test cases included isothermal flows of a single gas to check the velocity profiles, nonisothermal flows with insulated walls to check if the predicted exit temperature agrees with the one obtained from an overall heat balance, and isothermal diffusive flows of two gases to check the concentration profiles. Finally, simulations were performed using a single decomposition reaction to check if the code predicts expected trends in concentrations as the parameters of the model are varied. Overall atomic mass balances were also used to verify the predictions of the mass-transfer and kinetics part of the code.

Results and Discussion

Flow and temperature profiles

The effects of the thermal boundary conditions along the side walls on the flow and temperature profile in a reactor with a cool upper jet and a hot lower jet are shown in Figure 3. The temperature of the hot jet is 1,200 K and the upstream inlet velocity of both jets is 5 cm/s. For side walls cooled at 300 K, the pathlines of the gas plotted in Figure 3a indicate the presence of a strong buoyancy-driven recirculation just downstream of the region between the two jets. Such recirculations can complicate the kinetics experiments, because they can increase the residence time of reactants and products. These may subsequently diffuse from the recirculation into the reaction zone in the region between the jets and alter the observed concentrations. As a result, optimal operating conditions require that all existing recirculations are downstream from the sampling line and away from the region where reactions take place. The corresponding temperature profile, shown in Figure 3b, indicates that the temperature drops quickly in the downstream radial direction due to the heat losses from the side walls and the low heat capacity of the hydrogen gas. The predicted inlet temperature of the cool jet is higher than the ambient temperature, due to the natural boundary condition used in the heat-transfer model.

The fluid pathlines and isotherms for the case of insulated exit walls are shown in Figure 3c and 3d, respectively. The flow field is free of recirculations except possibly from small geometry-induced recirculations near the sharp corners at the points where the side walls meet the walls of the inlet tubes. Due to the absence of thermal losses along the side walls the temperature of the gas remains high in the exit region. By comparing Figures 3a and 3c it is apparent that the major cause of the recirculation shown in Figure 3a is the cooling of the side walls. The relative location of the two jets does not play a significant role as demonstrated in Figure 4, which shows the pathlines of the gas in a reactor with a hot upper jet, a cool lower jet, and all other operating conditions kept the same as in Figure 3a. A strong recirculation is still present in the exit region.

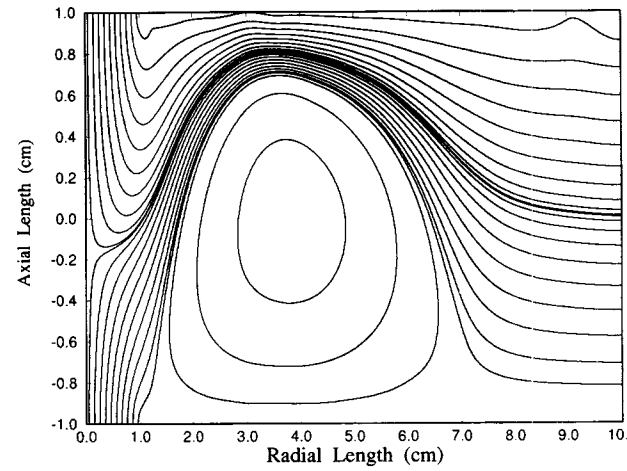

Figure 4. Pathlines of gas for hot upper jet.

Other conditions are as in Figure 3a.

To optimize the operating conditions with respect to the flow and temperature fields the following objectives were sought: (1) absence of recirculations inside and near the region between the two jets; (2) high temperatures in the middle region between the two jets to allow decomposition of the reactant; (3) low temperatures near the walls to avoid surface reactions. The case of water cooled side walls was considered, because insulated walls lead to high wall temperatures and are more likely to promote surface reactions.

The effect of the inlet flow rate and the operating pressure on removing buoyancy-driven recirculations from the region between the two jets is shown in Figure 5 for a hot-jet temperature of 900 K. At a low inlet velocity of 2 cm/s, a recirculation crosses the sampling line and penetrates into the region between the two jets, as shown in Figure 5a. This recirculation is effectively removed from that region by increasing the inlet velocity of the jets to 5 cm/s, as shown in Figure 5b. At high inlet velocities, forced convection dominates over natural convection and the recirculations are suppressed. The same result can be obtained by decreasing the operating pressure of the reactor from 1 to 0.5 atm while keeping the inlet velocity of the jets at 2 cm/s (computed at 300 K and 1 atm), as shown in Figure 5c. In this case the recirculation is suppressed due to a reduction in the density of the gas, which minimizes the effects of buoyancy.

The location of the stagnation point can be adjusted by changing the relative inlet flow rates of the two jets. This is shown in Figure 6 for three different velocities of the cool upper jet (5, 10, and 15 cm/s) while keeping the upstream inlet velocity of the hot lower jet constant at 5 cm/s. As the velocity of the upper jet increases the stagnation point is pushed down towards the hot lower jet. This technique can be used to change

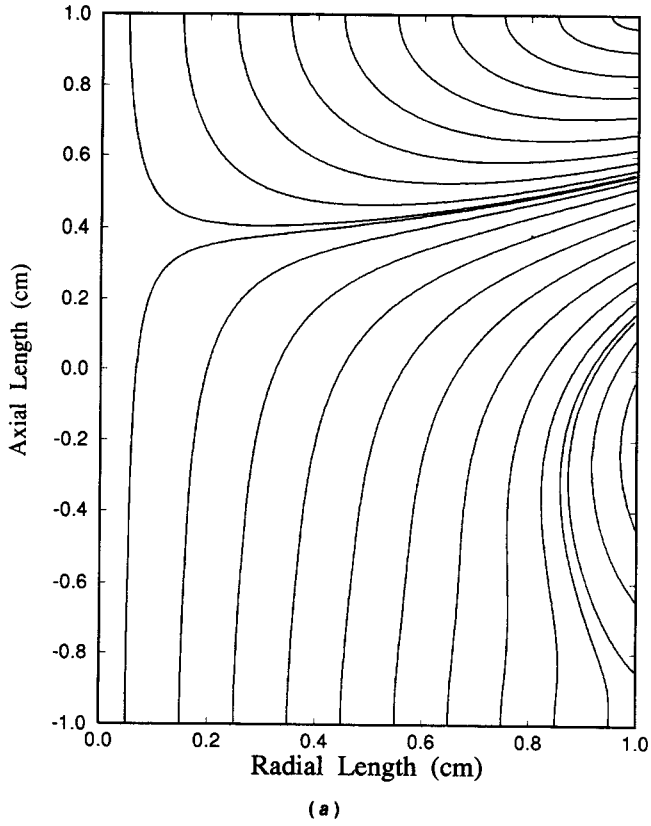

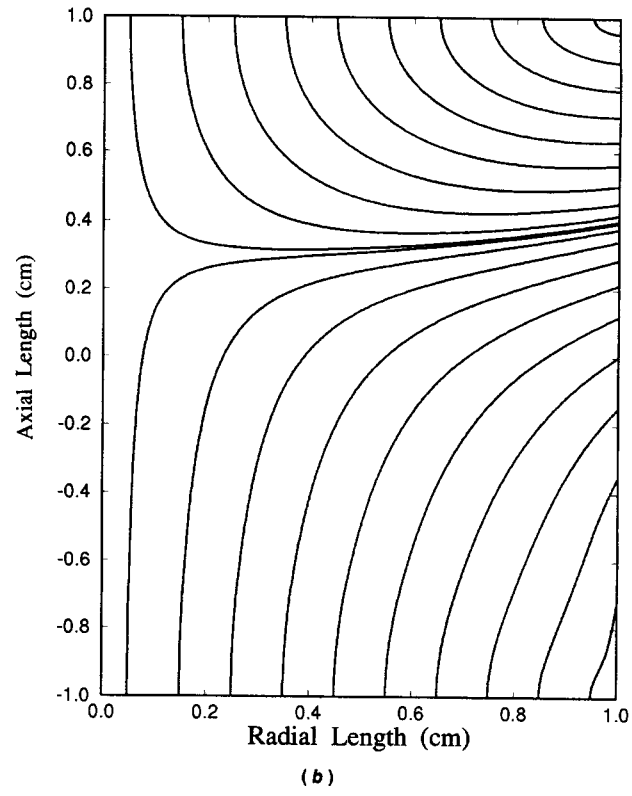

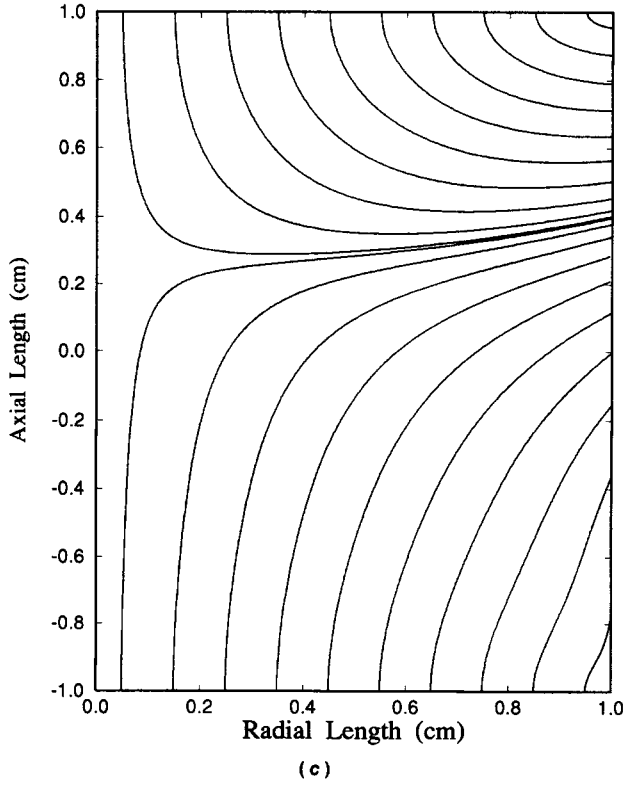

Figure 5. Plots of pathlines of gas demonstrating elimination of recirculations from region between jets by adjusting their inlet velocities or operating pressure.

(a) Recirculation penetrates into region between jets (lower right corner) when their inlet velocity is 2 cm/s (measured at 300 K and 1 atm), hot jet temperature is 900 K, and other conditions are as in Figure 3a; (b) recirculation is pushed out of this region by increasing velocity of jets to 5 cm/s; (c) recirculation is suppressed by decreasing operating pressure of reactor to 0.5 atm and keeping other conditions as in (a).

the location of the reaction zone when a single stationary probe is used, thus adding flexibility to the experiments. However, such adjustments must be done within certain limits to keep the reaction zone away from walls and avoid surface reactions. The case shown in Figure 6b is more attractive from this point of view compared to the other two cases, because the reaction zone is located near the middle of the gap.

Concentration profiles

The predicted temperature profile for the conditions cor-

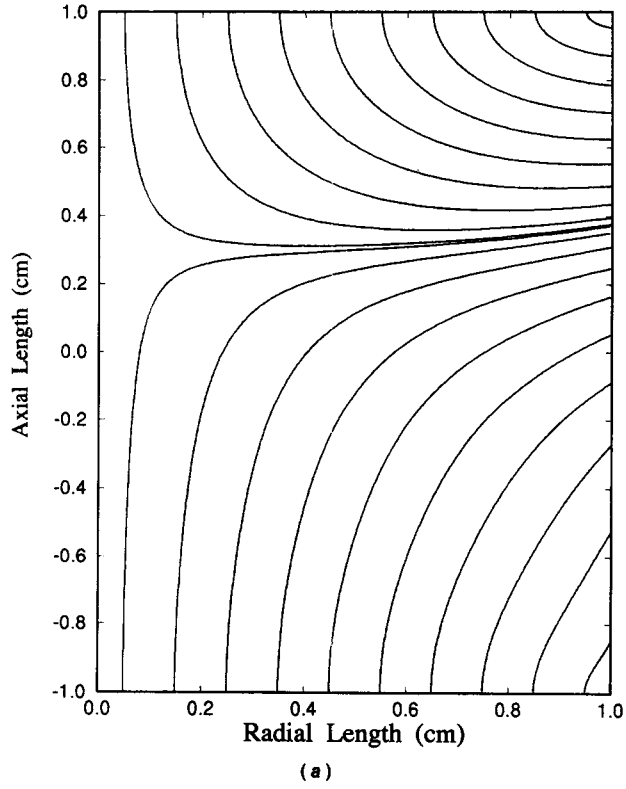

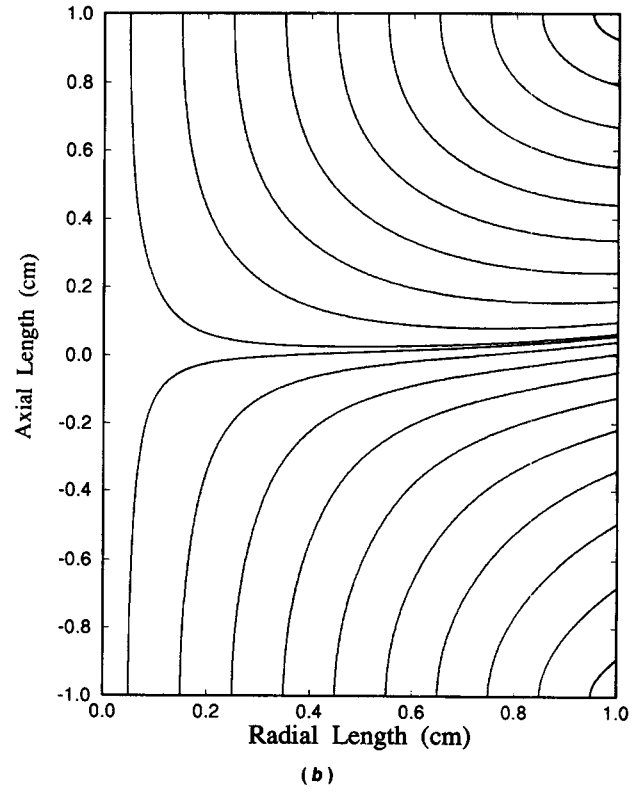

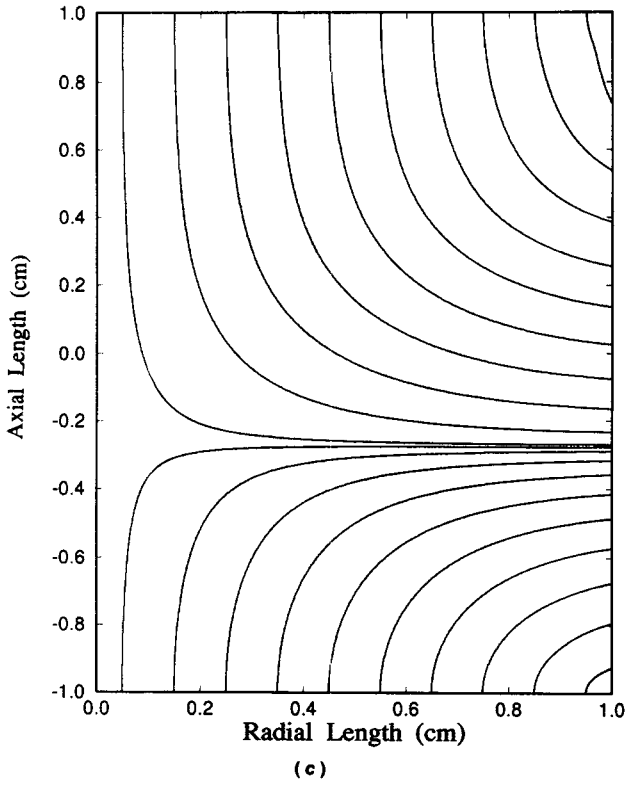

Figure 6. Effect of changing inlet velocity of cool upper jet on location of stagnation point (and reaction zone).

(a) Average inlet velocity of both jets is 5 cm/s; (b) inlet velocity of cool upper jet has been increased to 10 cm/s; (c) inlet velocity of cool upper jet has been increased to 15 cm/s. Other operating conditions are as in Figure 3a.

responding to Figure 6b together with the concentration profiles of TBA and the two hydrocarbon byproducts, i-C_4H_{10} and i-C_4H_8, are shown in Figure 7. In this case the velocity of the cool jet is high enough to keep the inlet relatively cool. This prevents the premature decomposition of TBA near the inlet, where surface reactions may take place on the walls. An interesting prediction is the apparent increase of the TBA concentration to a value higher than the inlet concentration in a region between the cool inlet and the hot reaction zone. This increase, which is about 10% in this case, is due to thermal diffusion of the TBA in the hydrogen carrier gas towards the cooler upper region of the reactor and away from the hot

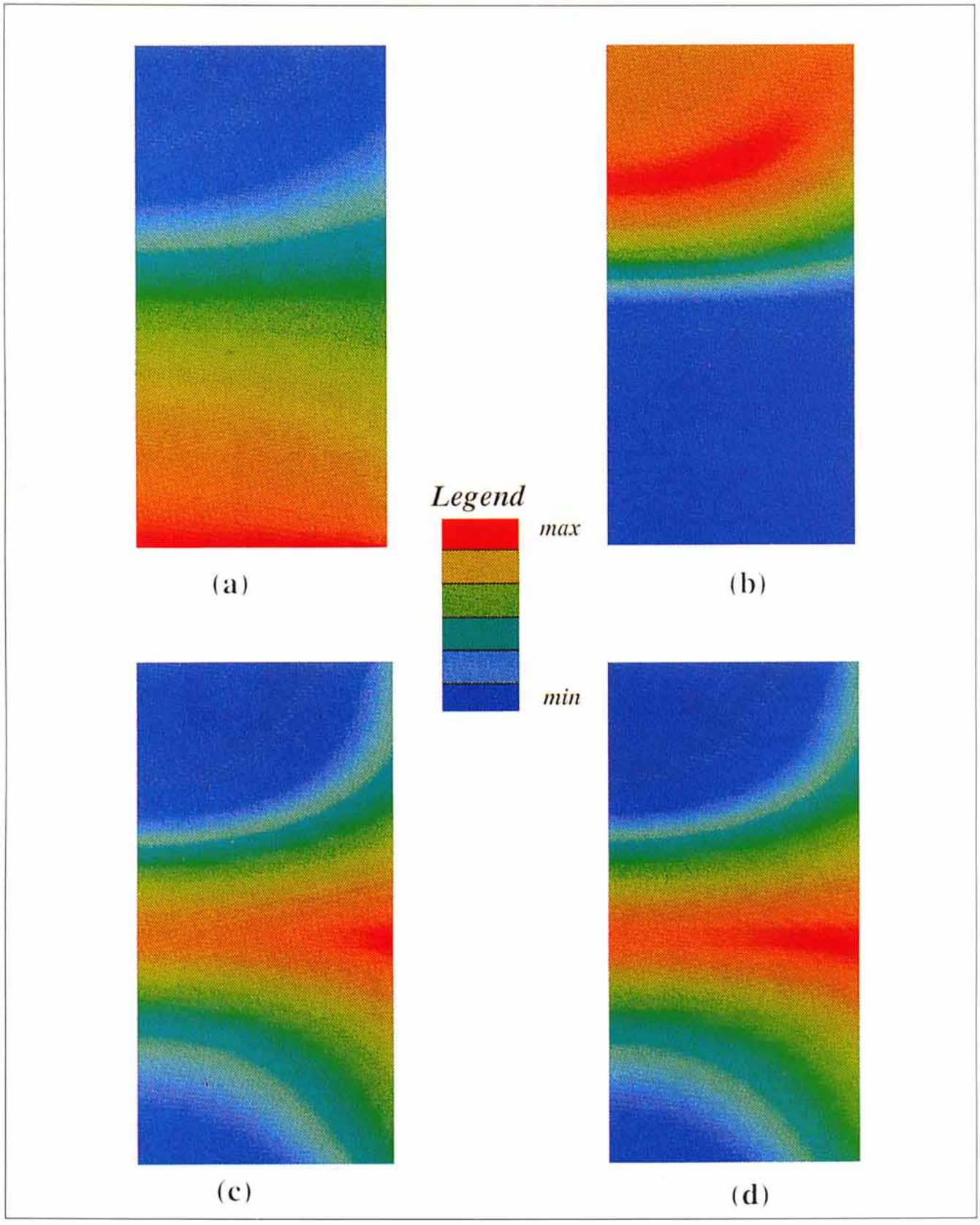

Figure 7. Temperature profile (a) and concentration profiles of TBA (b), $i-C_4H_{10}$ (c), and $i-C_4H_8$ (d) in region between two jets for operating conditions corresponding to Figure 6b.

Inlet mole fraction of TBA (upstream value) is 10^{-3} and is enriched to 1.1×10^{-3} by thermal diffusion just above the reaction zone. Maximum mole fraction of i-C_4H_{10} is 2.2×10^{-4} and that of i-C_4H_8 is 5×10^{-5}.

middle zone. Since forced convection and Fickian diffusion tend to push TBA downwards, the combination of the three effects results in the enrichment of TBA just above the reaction zone. The absence of reactions near the walls can be seen clearly in the concentration profiles of the two hydrocarbon byproducts shown in Figures 7c and 7d. In both cases the maximum concentration is near the middle of the gap, where these species are produced and subsequently diffuse by both Fickian and thermal diffusion to the neighboring regions. The concentration of i-C_4H_{10} is larger than that of i-C_4H_8 because of the faster kinetics of the intramolecular coupling reaction compared to the β-hydride elimination reaction.

For the optimal case shown in Figure 7, a probe located at the middle of the gap can be used to monitor the concentrations of the reactant and the products. The velocity of the cool upper jet can be subsequently adjusted to shift the reaction zone and enable data collection at different flow conditions. In a different set of experiments the velocities of both jets can be adjusted to keep the stagnation point near the middle of the gap. Since the residence time in the reaction zone can be manipulated by changing the velocities of the two jets, a sufficiently low residence time can always be achieved by using sufficiently high velocities. Thus, the onset of the decomposition of the reactant can be studied without any interference from secondary bimolecular reactions.

Parametric studies and optimal operating conditions

A parametric study was performed to identify the region of optimal operating conditions when the upstream velocities of the two jets are equal and the side walls are cool. The following criteria have been used:

(1) The concentration of TBA at the actual cool jet inlet is no less than 95% of its upstream value to avoid interference from surface reactions.

(2) The overall conversion of TBA in the reactor is larger than 15% to allow easy monitoring of the products.

(3) No recirculations penetrate into the region between the two jets.

A series of performance diagrams was developed using the Reynolds number and the Damköhler number for TBA decomposition defined as:

$$Da_{TBA} = \frac{(k_{h1} + k_{h2})D}{v_o} \tag{20}$$

Here k_{h1} and k_{h2} are the rate constants of the two parallel TBA decomposition steps, intramolecular coupling and the β-hydride elimination, respectively, computed at the average reactor temperature.

Figure 8 shows the performance diagrams for the reactor when the carrier gas is hydrogen and the cool jet is located either at the top (Figure 8a) or at the bottom (Figure 8b). The region of optimal operating conditions is above the 15% overall conversion curve and to the right of the other two curves. The location of the two jets appears to have only a small effect on the size of the optimal region. With a cool lower jet the optimal region is slightly more narrow than the one obtained with a cool upper jet. In both cases the conditions are optimal if the Damköhler number is larger than 100 and the Reynolds number

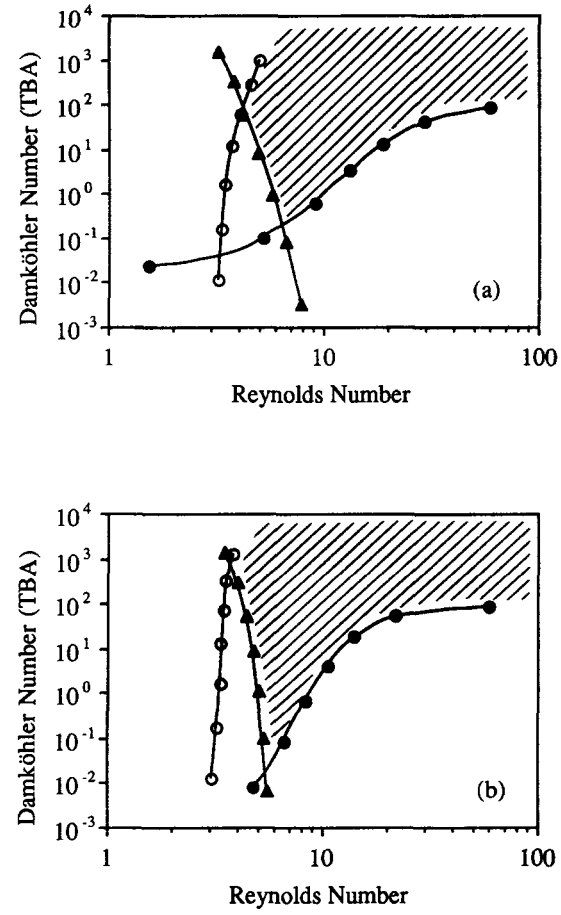

Figure 8. Performance diagram for TBA decomposition in hydrogen.

Operating pressure is 1 atm. Inlet mole fraction of TBA (upstream value) = 10^{-3}. Reactor size: $D = 2$ cm, $W = 2$ cm, and $L = 9$ cm. Inlet velocities of two jets are equal. (a) Hot jet is lower one; (b) hot jet is upper one; (o) mole fraction of TBA at actual inlet of cool jet equal to 95% of upstream value (larger to right of curve); (•) overall conversion of TBA is 15% (larger above the curve); (▲) no recirculations penetrate into region between two jets for operating conditions to right of this boundary. Shaded region corresponds to optimal conditions.

is larger than 6. There is also a minimum (critical) value of the Damköhler number and the Reynolds number below which the reactor cannot meet the above criteria. In this case, the critical value of the Damköhler number is 0.1 for a cool upper jet and 0.01 for a cool lower jet and the critical value of the Reynolds number is about 6 for both cases.

Figure 9 shows the effect of reducing the jet separation (gap) from 2 to 1 cm on the performance diagram shown in Figure 8a. When a smaller gap is used the recirculations are suppressed from the region between the two jets even at low Reynolds numbers due to the increased radial velocities. As a result, the region of optimal operating conditions becomes wider at low Damköhler and Reynolds numbers. When the gap was increased to 4 cm while keeping all other operating conditions constant, the buoyancy driven recirculations could not be eliminated from the region between the two jets except at high Reynolds numbers. However, at those conditions the residence time of the TBA in the reaction zone is short and its overall

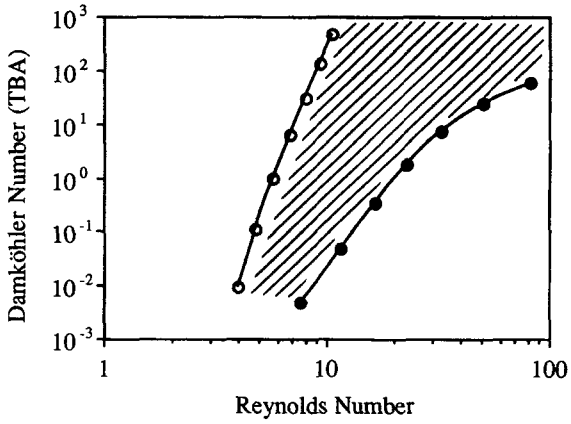

Figure 9. Effect of reducing gap size, *W*, from 2 cm to 1 cm on performance diagram shown in Figure 8a.

Symbols are as in Figure 8. Shaded region corresponds to optimal conditions.

conversion is always less than 15% for hot jet temperatures up to 1,100 K.

Finally, the effect of changing the carrier gas from hydrogen to nitrogen was investigated. When the operating conditions corresponding to Figure 8a were used, buoyancy driven recirculations penetrated into the region between the two jets, except at relatively high Reynolds numbers. This problem was solved by either reducing the gap or by reducing the operating pressure of the reactor. A performance diagram for TBA decomposition in nitrogen is shown in Figure 10 for an operating pressure of 0.1 atm. In this case the region of optimal operating conditions is large enough to allow data collection for determination of purely homogeneous kinetic parameters. It should be mentioned that falloff effects may lower the observed unimolecular decomposition rates at low operating pressures and should be taken into account, if they are significant. Such effects were neglected in the computation of the performance diagram shown in Figure 10.

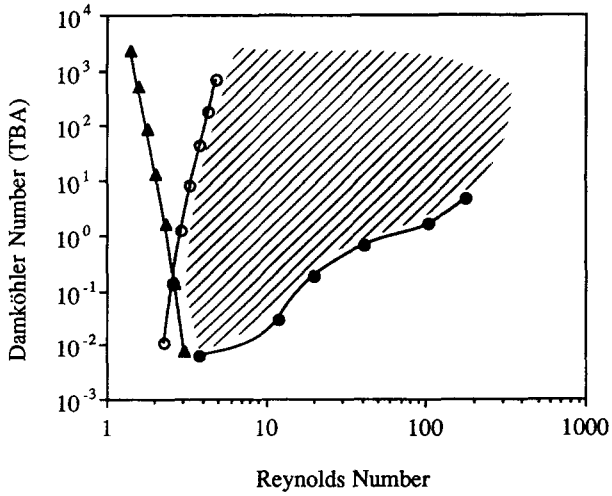

Figure 10. Performance diagram for TBA decomposition in nitrogen.

Operating pressure is 0.1 atm; inlet mole fraction of TBA is 10^{-3}; reactor size: $D=2$ cm, $W=2$ cm, and $L=9$ cm. Inlet velocities of two jets are equal. Hot jet is lower one. Symbols are as in Figure 8. Shaded region corresponds to optimal conditions.

Estimation of rate parameters

The proposed model can be used to obtain rate parameters of elementary reaction steps by comparing predicted and measured concentrations of species along the sampling line as well as at other locations inside the reaction zone (for example, along the axis of the reactor). Measurements of the temperature of the gas obtained by low profile thermocouples or by Raman spectroscopy can be used to improve the accuracy of the flow and heat-transfer part of the model. Furthermore, overall species balances in the reactor can be performed by measuring the composition of the outlet gas using gas chromatography or mass spectroscopy. The measured concentrations of gases at the exit can be compared to the ones predicted by the model to verify its validity.

If the decomposition of a new compound is studied, approximate values of the rate constants for unimolecular reactions can be usually obtained using thermochemical methods (Benson, 1976). A feasibility study can be subsequently performed using the proposed model to obtain the range of optimal operating conditions. If *a priori* estimates of the rate constants are not available, high flow rates can be initially used in the experiments to suppress decomposition reactions due to short residence times. Then, the flow rates can be lowered gradually until the first reaction byproducts are detected. Such experiments can be performed at different temperatures of the hot-jet, and rate constants for the onset of decomposition of the species can be fitted by comparing predicted concentrations to experimental ones. Finally, concentration measurements near the walls can be used to check for parasitic surface reactions, which are expected to produce increased amounts of byproducts near hot walls.

Conclusions

A new counterflow jet reactor has been designed for studying the purely homogeneous kinetics of endothermic reactions. The thermal decomposition of TBA has been used as an example in a feasibility study. A two-dimensional model of the reactor has been developed describing flow, heat, and mass transfer coupled with kinetics. Finite-element simulations were performed to predict the velocity, temperature, and concentration profiles in the reactor for a variety of operating conditions. Performance diagrams connecting the Damköhler and Reynolds numbers were developed to identify optimal operating conditions for gas-phase kinetic studies with minimal interference from surface reactions and from buoyancy-driven recirculations. By adjusting the flow rate of the two jets, both the residence time of species and the location of the reaction zone can be controlled. This allows the detection of the onset of homogeneous thermal decomposition of various species at pressures close to atmospheric and adds flexibility to the system, when moving the probe becomes impractical. The above features make the new reactor an attractive tool for homogeneous kinetic studies.

Acknowledgments

The authors gratefully acknowledge the financial support provided by the National Science Foundation (CTS-9010345 and CTS-9212682), by Eastman Kodak Company, and by the Center for Electronic and Electro-optic Materials at SUNY-Buffalo. The allocation of supercomputing resources by the Pittsburgh Supercomputing Center is also gratefully acknowledged. Finally, the authors are indebted to Mr. N. K. Ingle for many helpful discussions and for technical assistance in the computations and the graphics.

Notation

A_j = pre-exponential factor in the Arrhenius rate expression of the jth reaction
c = dimensionless total concentration in the gas phase
c_o = total concentration in the gas phase at inlet conditions T_o and p_o ($c_o = \rho_o/M$)
c_p = dimensionless specific heat of carrier gas
c_{po} = specific heat of carrier gas at T_o
C_{0i} = thermal diffusion constant of species i (Table 3)
C_{1i} = thermal diffusion constant of species i (Table 3)
C_{2i} = thermal diffusion constant of species i (Table 3)
D = diameter of inlet tubes
Da_j = Damköhler number of the jth reaction
D_i = dimensionless binary diffusion coefficient of the species i
D_{oi} = binary diffusion coefficient of the species i at 300 K and 1 atm (Table 3)
Da_{TBA} = Damköhler number for TBA decomposition
E_j = activation energy of the jth reaction
Fr = Froude number [$Fr = v_o^2/(gD)$]
g = gravitational acceleration
k = dimensionless thermal conductivity of carrier gas
k_{bj} = dimensionless rate coefficient of the backward jth reaction (normalized with k_{hj})
k_{fj} = dimensionless rate coefficient of the forward jth reaction (normalized with k_{hj})
k_{hj} = rate coefficient of the jth reaction computed at $(T_o + T_h)/2$
k_o = thermal conductivity of carrier gas at T_o
k_{Ti} = thermal diffusion ratio of species i
L = radial length of exit walls
m_j = order of the jth reaction
M = molecular weight of carrier gas
n = total number of reactions
N = total number of species
p = dimensionless pressure
p_o = inlet pressure
p_r = reactor pressure, atm
Pe = Peclet number for heat transfer [$Pe = (D\rho_o c_{po} v_o)/k_o$]
Pe_i = Peclet number for mass transfer of species i ($Pe_i = Dv_o/D_{oi}$)
r = dimensionless radial (horizontal) distance
R = ideal gas constant
Re = Reynolds number [$Re = (Dv_o\rho_o)/\mu_o$]
T = temperature, K
T_h = temperature of the hot jet, K
T_o = ambient temperature ($T_o = 300$ K) equal to upstream inlet temperature of the cool jet
v_{ho} = average upstream velocity of the hot jet measured at 300 K
v_o = average upstream velocity of the cool jet
v_r = dimensionless velocity of gas in the radial direction
v_z = dimensionless velocity of gas in the axial (vertical) direction
W = jet separation (gap)
x_i = mole fraction of species i
z = dimensionless axial (vertical) distance

Greek letters

α = aspect ratio ($\alpha = D/W$)
α_{Ti} = thermal diffusion factor of species i
ϵ/κ = Lennard-Jones parameter (Table 3)
Θ = dimensionless temperature ($\Theta = T/T_o$)
μ = dimensionless viscosity of carrier gas
μ_o = viscosity of carrier gas at T_o
ν_{ij} = stoichiometric coefficient of the ith species in the jth reaction
ρ = dimensionless density of carrier gas
ρ_o = density of carrier gas at inlet conditions T_o and p_o
σ = collision diameter (Table 3)

Subscripts

b = backward reaction
f = forward reaction
o = value of property at inlet conditions T_o and p_o

Literature Cited

Benson, S. W., *Thermochemical Kinetics*, Wiley, New York (1976).
Benson, S. W., and G. N. Spokes, "Very Low-Pressure Pyrolysis: I. Kinetic Studies of Homogeneous Reactions at the Molecular Level," *J. Amer. Chem. Soc.*, **89**, 2525 (1967).
Bird, R. B., W. E. Stewart, and E. N. Lightfoot, *Transport Phenomena*, Wiley, New York (1960).
Donnelly, V. M., J. A. McCaulley, and R. J. Shul, "Kinetics of Thermal Decomposition of Group-III Metal Alkyls on GaAs(100)," *Chemical Perspectives of Microelectronic Materials II*, L. V. Interrante et al., eds., Mat. Res. Soc. Symp. Proc., **204**, 15, Boston (1991).
Golden, D. M., G. N. Spokes, and S. W. Benson, "Very Low-Pressure Pyrolysis (VLPP): A Versatile Kinetic Tool," *Angew. Chem.* (int. ed.), **12**, 534 (1973).
Hirschfelder, J. O., C. F. Curtis, and R. B. Bird, *Molecular Theory of Gases and Liquids*, Wiley, New York (1967).
Jensen, K. F., "Micro-Reaction Engineering: Applications of Reaction Engineering to Processing of Electronic and Photonic Materials," *Chem. Eng. Sci.*, **42**, 923 (1987).
Kuech, T. F., "Metal-Organic Vapor Phase Epitaxy of Compound Semiconductors," *Mat. Sci. Rep.*, **2**, 1 (1987).
Larsen, C. A., N. I. Buchan, and G. B. Stringfellow, "Reaction Mechanisms in the Organometallic Vapor Phase Epitaxial Growth of GaAs," *Appl. Phys. Lett.*, **52**, 480 (1988).
Larsen, C. A., N. I. Buchan, and G. B. Stringfellow, "Decomposition Mechanisms of Tertiarybutylarsine," *J. Cryst. Growth*, **94**, 663 (1989).
Lee, P. W., T. R. Omstead, D. R. McKenna, and K. F. Jensen, "*In Situ* Mass Spectroscopy Studies of the Decomposition of Organometallic Arsenic Compounds in the Presence of $Ga(CH_3)_3$ and $Ga(C_2H_5)_3$," *J. Cryst. Growth*, **93**, 134 (1988).
Lückerath, R., P. Tommack, A. Hertling, H. J. Koss, P. Balk, K. F. Jensen, and W. Richter, "CARS *In Situ* Diagnostics in MOVPE: The Thermal Decomposition of AsH_3 and PH_3," *J. Cryst. Growth*, **93**, 151 (1988).
Lum, R. M., J. K. Klingert, and M. G. Lamont, "Use of Tertiarybutylarsine in the Metalorganic Chemical Vapor Deposition Growth of GaAs," *Appl. Phys. Lett.*, **50**, 284 (1987).
Mountziaris, T. J., and K. F. Jensen, "Gas-Phase and Surface Reaction Mechanisms in MOCVD of GaAs with Trimethyl-Gallium and Arsine," *J. Electrochem. Soc.*, **138**, 2426 (1991).
Mountziaris, T. J., S. Kalyanasundaram, and N. K. Ingle, "A Reaction-Transport Model of GaAs Growth by Metalorganic Chemical Vapor Deposition Using Trimethyl-Gallium and Tertiary-Butyl-Arsine," *J. Cryst. Growth*, **131**, 283 (1993).
Nishizawa, J., T. Kurabayashi, H. Abe, and A. Nozoe, "Mechanism of Surface Reaction in GaAs Layer Growth," *Surf. Sci.*, **185**, 249 (1987).
Perry, R. H., and C. H. Chilton, *Chemical Engineer's Handbook*, 5th ed., McGraw-Hill, New York (1974).
Reid, R. C., J. M. Prausnitz, and T. K. Sherwood, *The Properties of Gases and Liquids*, McGraw-Hill, New York (1977).
Robinson, P. J., and K. A. Holbrook, *Unimolecular Reactions*, Wiley-Interscience, London (1972).
Roegnik, K. F., K. F. Jensen, and R. W. Carr, "Rice-Ramsperger-Kassel-Marcus Theoretical Prediction of High-Pressure Arrhenius

Parameters by Nonlinear Regression: Application to Silane and Disilane Decomposition," *J. Phys. Chem.*, **91**, 5732 (1987); errata in *J. Phys. Chem.*, **92**, 4254 (1988).
Safvi, S. A., and T. J. Mountziaris, "Gas Phase Decomposition Kinetics of MOVPE Precursors in a Counterflow Jet Reactor," *Chemical Perspectives of Microelectronic Materials III*, C. R. Abernathy et al., eds., Mat. Res. Soc. Symp. Proc., 282 (1993).
Seshadri, K., C. Trevino, and M. D. Smooke, "Analysis of the Structure and Mechanisms of Extinction of a Counterflow Methanol-Air Diffusion Flame," *Combust. Flame*, **76**, 111 (1989).
Strang, G., and G. Fix, *An Analysis of the Finite Element Method*, Prentice Hall, Englewood Cliffs, NJ (1973).
Stringfellow, G. B., *Organometallic Vapor-Phase Epitaxy: Theory and Practice*, Academic Press, Boston (1989).
Tamaru, K., "The Decomposition of Arsine," *J. Phys. Chem.*, **59**, 777 (1955).
Westmoreland, P. R., J. B. Howard, J. P. Longwell, and A. M. Dean, "Prediction of Rate Constants for Combustion and Pyrolysis Reactions by Bimolecular QRRK," *AIChE J.*, **32**, 1971 (1986).
Zachariah, M. R., and H. G. Semerjian, "Simulation of Ceramic Particle Formation: Comparison with In-Situ Measurements," *AIChE J.*, **35**, 2003 (1989).

Manuscript received June 28, 1993, and revision received Oct. 22, 1993.